


RESEARCH ARTICLE

Characterization of an extremophile bacterial acid phosphatase derived from metagenomics analysis

Maria-Isabel Recio¹ | Jesús de la Torre¹ | Abdelali Daddaoua²  |
Zulema Udaondo³  | Estrella Duque¹ | José Antonio Gavira⁴ |
Carmen López-Sánchez⁴ | Juan L. Ramos¹ 

¹Consejo Superior de Investigaciones Científicas, Estación Experimental del Zaidín, Department of Environmental Protection, Granada, Spain

²Department of Biochemistry and Molecular Biology II, Pharmacy School, Granada University, Granada, Spain

³Department of Biomedical Informatics, College of Medicine, University of Arkansas for Medical Sciences, Little Rock, Arkansas, USA

⁴Consejo Superior de Investigaciones Científicas, Instituto de Ciencias de la Tierra, Granada, Spain

Correspondence

Juan-Luis Ramos, Estación Experimental del Zaidín, Department of Environmental Protection, 18008 Granada, Spain.
Email: juanluis.ramos@eez.csic.es

Funding information

Ministerio de Ciencia e Innovación, Grant/Award Number: EJPSoIL862695, PID2021123469OBI00, PREPSOIL (HE/CL5SOILM/0102) and TED2021129632BI00

Abstract

Acid phosphatases are enzymes that play a crucial role in the hydrolysis of various organophosphorous molecules. A putative acid phosphatase called FS6 was identified using genetic profiles and sequences from different environments. FS6 showed high sequence similarity to type C acid phosphatases and retained more than 30% of consensus residues in its protein sequence. A histidine-tagged recombinant FS6 produced in *Escherichia coli* exhibited extremophile properties, functioning effectively in a broad pH range between 3.5 and 8.5. The enzyme demonstrated optimal activity at temperatures between 25 and 50°C, with a melting temperature of 51.6°C. Kinetic parameters were determined using various substrates, and the reaction catalysed by FS6 with physiological substrates was at least 100-fold more efficient than with *p*-nitrophenyl phosphate. Furthermore, FS6 was found to be a decamer in solution, unlike the dimeric forms of crystallized proteins in its family.

INTRODUCTION

Phosphorous is an essential component of all living organisms, and cells have developed mechanisms to acquire inorganic phosphate for various biological processes. In addition, phosphorous is also a limiting nutrient, the second after N in soil, for plant growth and productivity (Attwood, 2013; Bonneau et al., 2013; Ramos, 2022; Blank, 2023). Phosphatases play a crucial role in hydrolyzing organophosphorus

compounds into assimilable inorganic phosphate to sustain the phosphorus cycle. They are also involved in cell signalling and protein modification. Acid phosphatases, which exhibit optimal activity at pH 5–6, and alkaline phosphatases, with optimal activity at pH 7.5–8.5, are the two main groups of phosphatases (Dick et al., 2000; Gandhi & Chandra, 2012; Li et al., 2007). Acid phosphatases are prevalent in soils and the rhizosphere, and their role in the phosphorus cycle has been underestimated (Margalef et al., 2017,

Abbreviations: DTT, dithiothreitol; ΔH , enthalpy change of binding; ITC, isothermal titration calorimetry; PNPP, *p*-nitrophenyl phosphate.

Maria-Isabel Recio and Jesús de la Torre contributed equally to this work and should be considered as first co-authors.

This is an open access article under the terms of the [Creative Commons Attribution-NonCommercial-NoDerivs](https://creativecommons.org/licenses/by-nc-nd/4.0/) License, which permits use and distribution in any medium, provided the original work is properly cited, the use is non-commercial and no modifications or adaptations are made.

© 2024 The Authors. *Microbial Biotechnology* published by Applied Microbiology International and John Wiley & Sons Ltd.

2021; Wang et al., 2018). To study acid phosphatases further, PROSITE “generalized” profiles were constructed and used to identify bacterial acid phosphatases in custom metagenome and genome databases. Three families of bacterial acid phosphatases were identified, known as classes A, B, and C. Class B acid phosphatases are associated with pathogens, while types A and C are widely distributed (Neal et al., 2018; Udaondo et al., 2020). Acid phosphatases have a broad range of substrates and can be located either extracellularly or intracellularly, playing important roles in signal transduction pathways and nucleic acid biosynthesis (Lidbury et al., 2016; Lidbury et al., 2022; Udaondo et al., 2020; Wang et al., 2018).

In the study by Udaondo et al. (2020), several unknown acid phosphatases, identified in genomic and metagenomic databases, were expressed in *Escherichia coli* to confirm their activity. Most of the cloned acid phosphatases exhibited optimal activity at acidic pH using *p*-nitrophenyl phosphate (PNPP) as a substrate. However, FS6, a type C acid phosphatase, showed high activity across a wide pH range of 3.5–8.5, indicating its unique properties. FS6 has been purified and further characterized, confirming its extremophile properties and ability to function effectively between 20 and 50°C. The enzyme has been characterized kinetically and physico-chemically, revealing its decameric quaternary structure in solution, unlike the dimeric forms observed in crystallized class C acid phosphatases.

EXPERIMENTAL PROCEDURES

Bacterial strains, plasmids, and culture media

The *E. coli* BL21 (DE3) strain was utilized for protein overexpression (Hananhan et al., 1983), and *Escherichia coli* DH5 α (Studier et al., 2009) was used for cloning. Bacterial cells were grown in LB medium at temperatures ranging from 18 to 37°C. Plasmids employed or constructed in this study are shown in Table S1. When necessary, kanamycin (Km) or ampicillin (Ap) were added at a concentration of 25 or 100 μ g/mL, respectively.

Protein purification

For protein purification, cells (1–2 g) were resuspended in 25 mL of buffer A (40 mM MES, 40 mM HEPES, 40 mM acetic acid, pH 8.0, 500 mM NaCl, 1 mM dithiothreitol (DTT), and 10% (v/v) glycerol) supplemented with an EDTA-free protease inhibitor mixture. Cell lysis was achieved through three passes using a French Press at a pressure of 1000 p.s.i. The resulting cell suspension

was then centrifuged at 6000g for 30 min. The pellet was discarded, and the supernatant was filtered using sterile 0.22- μ m filters before being loaded onto a 5 mL His-Trap chelating column (GE Healthcare, St. Gibes, UK). The proteins were eluted using a gradient of 0–500 mM imidazole in buffer B (i.e., Buffer A plus 500 mM imidazole). The purity of the eluted protein fractions was assessed using 12% (w/v) SDS-PAGE gels. Homogeneous protein fractions were dialysed overnight against buffer A but with 150 mM NaCl instead of 500 mM and four different pH, namely, 4, 5.5, 7, and 8.5.

Enzymatic activity assays

Acid phosphatases hydrolyse the substrate PNPP, an artificial phosphate ester, producing phosphate and *p*-nitrophenol as products. The standard assay for phosphatase activity was conducted in 0.1 mL of HAM (40 mM HEPES, 40 mM acetic acid, and 40 mM MES) poly-buffer with a buffering capacity ranging from pH 3.5 to pH 8.5. The standard assay mixture contained 0.1–1 μ M of the FS6 enzyme and 0.22 mM of the substrate. The reaction product (*p*-nitrophenol) was measured spectrophotometrically at 405 nm using a Tecan Sunrise plate reader (Tecan Austria GmbH). The effect of temperature and pH on the activity of the enzyme was evaluated in the standard assay mixture at specified temperatures and pH values. For temperature assays, the reaction mixture was incubated at 20, 30, 40, 50, 60, 70, and 80°C. Enzyme activity at different pH values was determined as described above at two different temperatures (30 and 50°C) and at pH values of 3.5, 4.5, 5.5, 6.5, 7.5, and 8.5. The reaction was halted by adding 100 μ L of 0.5 M NaOH and 800 μ L of distilled H₂O. For kinetics analysis, increasing concentrations of PNPP or several nucleoside monophosphates (adenosine 5'-monophosphate (5'-AMP), guanosine 5'-monophosphate (5'-GMP), and uridine 5'-monophosphate (5'-UMP)) ranging from 0 to 0.22 mM were used. Kinetic data were analysed using both the Michaelis–Menten equation and the Lineweaver–Burk plot.

Isothermal titration calorimetry (ITC) assays

Microcalorimetric phosphatase activity assays were conducted at 25°C using a VP-microcalorimeter (Microcal, Amherst, Massachusetts, USA; Todd & Gomez, 2001; Bianconi, 2003; Krell, 2008; Zambelli, 2019). The purified phosphatase and substrate solutions were dialysed against a buffer made of 40 mM MES, 40 mM HEPES, 40 mM acetic acid, 150 mM NaCl, 1 mM DTT, and 10% [v/v] glycerol at pH 4, 5.5, 7, and

8.5. Substrates were prepared in the same buffer. The titration involved injecting 10 μL of 500 μM substrate solution into 0.1–1 μM of purified FS6 acid phosphatase in the same buffer. Control experiments consisted of injecting the substrate solution into the dialysis buffer. Raw titration data were normalized for concentration and corrected for dilution effects before analysis using the 'Enzyme kinetics—single injection model' of the MicroCal PEAQ-ITC analysis software. The parameter ΔH (reaction enthalpy) was determined through curve fitting (Abadou & Labdury, 2006).

Analytical ultracentrifugation

An Optima XL-I analytical ultracentrifuge (Beckman-Coulter, Palo Alto, CA) equipped with a UV-visible absorbance detection system was employed. Experiments were conducted at 20°C using an AnTi50 rotor, and absorbance scans were recorded at 280 nm. Sedimentation velocity experiments were performed using epon-charcoal standard double sector centre-pieces (12-mm optical path) at a speed of 48,000 rpm. Sedimentation coefficient distributions were determined by performing direct linear least-squares boundary fitting of the sedimentation velocity profiles using SEDFIT software (Brown & Schuck, 2008; Zhao et al., 2010). SEDNTERP software (Philo, 2023) was employed to correct S values to standard conditions (20°C and water). The apparent weight-average buoyant molecular weight of the protein samples was determined by fitting a single-species model to the experimental data using a MATLAB program based on the conservation of a signal algorithm. The corresponding protein molecular weights were calculated using a protein partial specific volume of 0.725 cm^3/g .

Electron microscopy of the FS6 protein

Samples of FS6 in the HAM poly-buffer at various concentrations (1–5 μg per mL) were deposited as 5- μL drops on metallic grids. The samples were then treated with uranyl acetate, dried, and heat-fixed. An UltraHigh Resolution HRTEM TITAN instrument at the Center of Scientific Instrumentation at the University of Granada was utilized for sample analysis. The obtained images were processed using the ImageJ program.

Differential scanning Fluorimetry (DSF)

Thermal denaturation assays were conducted using a MyIQ2 Real-Time PCR instrument (Fernández

et al., 2019). Twenty five μL of a preparation at 5, 10 and 20 μM of FS6 supplemented with 5x SYPRO orange in HAM buffer at pH 5.5 was heated from 23 to 85°C with a heating rate of 1°C per minute. The fluorescence emission was monitored over time. Finally, the melting temperatures (T_m) were calculated using Bio-Rad iQ5 software.

Plasmid DNA extraction and generation of mutant proteins FS6(D58A), FS6(D60A), FS6(D207A) and FS6 (D211A)

To obtain highly pure plasmid DNA, the NZYMiniprep commercial kit (NZYTech) was used according to the manufacturer's instructions. Cells from a 24-h culture in LB medium supplemented with the appropriate antibiotic were collected by centrifugation (2 mL) at 10,000 g for 1 min.

To generate point mutations, replacing aspartic acid at positions 58, 60, 207, and 211 with alanine residues, the pET28(b)::FS6 plasmid served as a template. A 196-bp fragment (amplicon 1F) was amplified by PCR using the FS6 Fw NdeI and FS6 Rv1 oligonucleotides (Table S2). An 846-bp fragment was amplified using the FS6 Fw1 and FS6 Rv EcoRI oligonucleotides (amplicon 1R). Similarly, a 403-bp fragment (amplicon 2F) was generated using the FS6 Fw (NdeI) and FS6 Rv2 oligonucleotides, and a 633-bp fragment (amplicon 2R) was produced using the FS6 Fw2 and FS6 Rv (EcoRI) oligonucleotides. A 194-bp fragment was amplified by PCR using the FS6 Fw NdeI and FS6 Rv3 (amplicon 3F) and a 858-bp fragment was amplified using the FS6 Fw3 and FS6 Rv EcoRI oligonucleotides (amplicon 3R). A 651-bp fragment (amplicon 4F) was generated using the FS6 Fw (NdeI) and FS6 Rv4 oligonucleotides, and a 398-bp fragment (amplicon 4R) was produced using the FS6 Fw4 and FS6 Rv (EcoRI) oligonucleotides. These fragments were then used as templates for another overlapping amplification. Amplicons 1F and 1R, with FS6 Fw NdeI and FS6 Rv EcoRI oligonucleotides, generated the FS6(D60A) insert with the corresponding mutation, respectively. Amplicons 2F and 2R, with the FS6 Fw NdeI and FS6 Rv EcoRI oligonucleotides, respectively, produced the FS6(D207A) insert with the corresponding mutation. Amplicons 3F and 3R, with FS6 Fw NdeI and FS6 Rv EcoRI oligonucleotides, respectively, generated the FS6(D58A) insert with the corresponding mutation. Amplicons 4F and 4R, with the FS6 Fw NdeI and FS6 Rv EcoRI oligonucleotides, respectively, produced the FS6(D211A) insert with the corresponding mutation (Table S2). The amplified fragments were ligated into the pGEM-T vector to obtain the recombinant pGEM-T::FS6 (D60A), pGEM-T::FS6(D207A), pGEM-T::FS6(D58A),

and pGEM-T::FS6(D211A) plasmids. After confirming the constructs through Sanger sequencing, the different gene variants were subcloned into pET28(b) using the endonuclease recognition sites NdeI and EcoRI for expression and further characterization of the encoded mutant protein.

Substrate profile of FS6

To determine the substrate profile of the FS6 protein, we quantified the concentration of orthophosphate released from a range of organophosphorous chemicals available in the Phenotype MicroArrays™ technology PM4A plate (Biolog, Hayward, CA, USA). Orthophosphate was quantified using the “Malachite Green Phosphate Assay” kit from Sigma-Aldrich. The assays were done at four different pH: 4, 5.5, 7, and 8.5. The quantification is based in complex formation between malachite green, molybdate, and free orthophosphate, and the complex was measured using a TECAN Sunrise multi-well plate reader at a wavelength of 660 nm. A positive reaction for FS6 was considered when the amount of phosphate released exceeded 10 μ M.

RESULTS

The FS6 gene encodes a 335-amino acid protein with a molecular mass of approximately 38 kDa, which falls within the general molecular mass range of class C acid phosphatases (25–38 kDa) (Rossolini et al., 1998). Udaondo et al. (2020) derived a consensus sequence from the multi-alignment of 1500 class C acid phosphatases. When we compared the FS6 sequence to the consensus class C-derived sequence, it was found that 30% of the residues in the FS6 protein were identical to those in the consensus sequence (Figure S1). To purify the FS6 protein, a codon-optimized FS6 gene was designed and cloned in pET28(b) for expression in *E. coli*, resulting in the whole protein-coding region downstream from a His tag sequence in the pET28(b) plasmid. Induction assays were performed at different temperatures and with various IPTG concentrations. Cell-free extracts were prepared as described in the *Experimental Procedures* section and analysed by SDS-PAGE. The highest protein yields were obtained when bacteria were grown at 30°C with 0.5 mM IPTG. Subsequently, cell-free extracts were prepared, and the recombinant His-FS6 fusion protein was purified to homogeneity using an FPLC system with a nickel affinity column. As expected, the purified protein exhibited phosphatase activity with PNPP as a substrate, and in SDS-PAGE gels, a single band of approximately 38 kDa was observed.

Effect of pH and temperature on FS6 enzyme activity

Initially, we assessed the functional pH range of the protein using PNPP as a substrate. We employed the HAM poly-buffer, enabling measurement of activity within pH 3.5 to 8.5. At 30°C, the protein displayed maximal activity between pH 4.5 and 7.5, retaining approximately 80% activity at pH 3.5 and 40% at pH 8.5 (Figure 1). These findings suggest that FS6 exhibits unusual acid phosphatase characteristics, differing from the bell-shaped pH rate profile typically observed in acid phosphatases according to Van Etten (1982) and other researchers (Shi et al., 2022; Du Plessis et al., 2002; Reilly et al., 2009). This distinct behaviour classifies FS6 as a unique class C acid phosphatase.

Considering that most acid phosphatases exhibit optimum activity at pH 5.5, we selected this pH to assess protein activity within a temperature range of 20–80°C. We observed that the enzyme exhibited near-maximal activity between 30 and 50°C, with a 50% decrease at 20°C and 70% decrease at 60°C (Table 1). To further analyse the stability of the protein at different temperatures, we conducted differential scanning fluorometry (DSF) assays. These assays, performed at three different protein concentrations, revealed a melting temperature of approximately 51°C (Figure 2), indicating

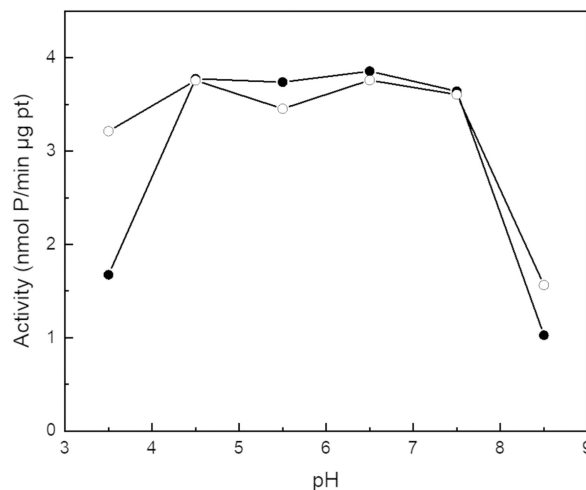


FIGURE 1 Activity Profile of FS6 Acid Phosphatase as a Function of pH. The activity profile of FS6 acid phosphatase is depicted as a graph showing its enzymatic activity at various pH values. The assay mixture used in this experiment was prepared according to the protocols described in the *Experimental procedures* section. The pH of the mixture was adjusted using NaOH. The enzyme activity was measured at two different temperatures: 30°C (shown as closed circles) and 50°C (shown as open circles). The substrate used for the enzymatic reaction was PNPP, and the enzyme activity is presented as the amount of phosphate released per minute per microgram of protein. The assays were done at least three times, and the standard deviation was less than 15% of the average values.

TABLE 1 Effect of the incubation temperature on the activity of the FS6 protein.

Temperature (°C)	Activity (%)
20	53 +/-20
30	97+/-10
40	92+/-12
50	100+/-15
60	29+/-9
70	9+/-9
80	5+/-1

Note: The assay was performed in the standard reaction mixture with PNPP as a substrate. 100% activity represents the release of 10 nmoles P per minute and microgram of protein. The assays were performed in triplicate. The standard error is given.

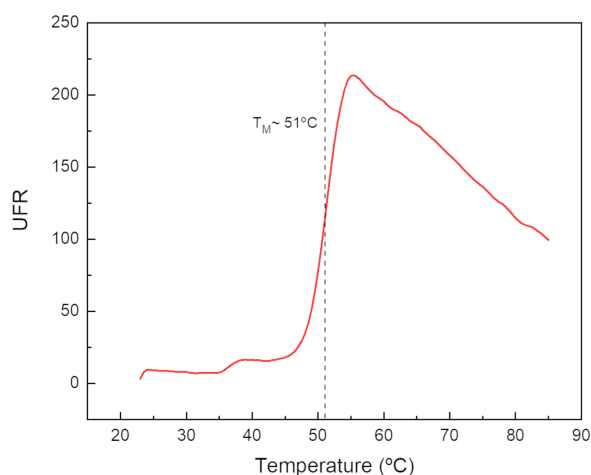


FIGURE 2 Thermal Unfolding Behaviour of FS6 Acid Phosphatase. This figure illustrates the impact of incubation temperature on the thermal stability of FS6 acid phosphatase. The assay evaluates the stability of the enzyme FS6 (5 μ M) in HAM buffer at pH5.5. Similar results were obtained when using 1 or 10 μ M of the protein. The melting temperature was determined using the Bio-Rad iQ5 software.

the thermophilic nature of the protein and its ability to maintain activity at 50°C.

Subsequently, we investigated the effect of pH at 50°C and found that the activity profile at 30 and 50°C was similar (Figure 1). However, at pH3.5 and 50°C, the activity was approximately 45% of the maximal activity, and at pH8.5 the enzyme activity was approximately 20% of the maximal one. These results indicate that FS6 is an extremozyme class C acid phosphatase, as it functions over a wide pH and temperature range.

Studies on different classes of acid phosphatases have suggested the involvement of metals in catalysis, protein–substrate interactions, or protein stabilization (Mitić et al., 2006; Reilly et al., 2009). To explore this aspect, we dialysed the purified FS6 enzyme against a metal-free buffer containing 1 mM EDTA at pH5.5. Interestingly, the EDTA-treated enzyme retained

around 30% of its maximal activity. Subsequently, we incubated the EDTA-treated enzyme with 1 μ M Mg^{2+} , Ca^{2+} , Cd^{2+} , Cu^{2+} , Zn^{2+} , Mn^{2+} , Ni^{2+} , and Co^{2+} for 30 min, followed by activity assays at pH5.5 and 25°C. The results indicated that Cu^{2+} , Mn^{2+} , and Mg^{2+} fully restored enzyme activity, while other divalent cations such as Ni^{2+} , Co^{2+} , and Ca^{2+} only restored partially the activity (Table S3). Furthermore, DSF assays were also conducted in the presence of 1 mM different metals, and the assay revealed a melting temperature of 51°–54°C (Table S3), suggesting that metals are not involved in protein stabilization but rather in catalysis, consistent with the findings of other class C phosphatases as it is the case for acid phosphatase P4 (Felts et al., 2007). The stimulation of activity of class C acid phosphatase by a diverse set of metals (such as Mg^{2+} , Ca^{2+} , Zn^{2+} , and Ni^{2+}) has been reported for class C acid phosphatases from *Propionibacterium*, *Clostridia*, and other organisms. Our DSF analysis supports that this phenomenon is associated with catalytic activity rather than structural stability as reported for other phosphatases (Gottesman et al., 2020).

The substrate range of the FS6 enzyme and kinetic parameters

Acid phosphatases are known for their broad substrate specificity (Attwood, 2013; Kaur et al., 2007; Lidbury et al., 2022; Rigden et al., 2001; van Etten & Waymack, 1991). To assess the activity of FS6 with a wide range of substrates, we utilized the PM4A Biolog platform and several other substrates (see Table 2), and the release of phosphate from a wide range of organophosphorus compounds at pH4, 5.5, 7, and 8.5 at 25°C was measured. Our results confirmed that FS6 released phosphate over a wide pH range when using PNPP as a substrate. Similarly, various 5'- and 3'-nucleoside phosphates, as well as ribose-5-phosphate, showed activity across multiple pH values. However, with cytidine-2'-monophosphate, guanosine-2',3'-cyclic monophosphate and ADP the FS6 protein displayed activity preferentially at pH5.5 and 7, respectively. Several compounds, including ATP, pyridoxal-P, adenosine 2'-monophosphate, glucose-6-phosphate, and α -glycerol phosphate, were only hydrolysed at pH5.5 (Table 2). These results highlight the broad substrate specificity of FS6 as an acid phosphatase, particularly at acidic pH, while showing a more restricted range of substrates at neutral/alkaline pH.

Given the characteristics of FS6, we proceeded to determine its kinetic parameters with PNPP, 5'-AMP, 5'-GMP, and 5'-UMP at pH4, 5.5, and 7, respectively, both at 25°C and 50°C. Substrate hydrolysis rates followed Michaelis–Menten kinetics, and V_{max} and K_m values were obtained from Lineweaver–Burk double reciprocal

TABLE 2 Substrate profile of the FS6 protein at different pH.

Phosphorus substrate	pH4	pH5.5	pH7	pH8.5
Thiophosphate	<10	10	<10	<10
Dithiophosphate	10	<10	<10	<10
D,L- α -glycerol phosphate	<10	27	10	<10
Adenosine-2'-monophosphate	<10	16	<10	<10
Cytidine-2'-monophosphate	11	36	36	<10
Adenosine-3'-monophosphate	39	42	53	36
Guanosine-3'-monophosphate	20	34	30	12
Uridine-3'-monophosphate	<10	31	<10	<10
Thymidine-3'-monophosphate	19	42	38	33
Adenosine-5'-monophosphate	35	44	52	29
Guanosine-5'-monophosphate	29	35	55	32
Cytidine-5'-monophosphate	25	35	41	25
Uridine-5'-monophosphate	28	26	47	32
Thymidine-5'-monophosphate	23	37	46	38
Guanosine-2'-3' cyclic monophosphate	12	21	27	<10
O-phospho-D-Tyrosine	<10	26	<10	<10
O-phospho-L-Tyrosine	<10	32	<10	<10
Phosphocreatine	<10	15	<10	<10
Phosphoryl choline	<10	13	<10	<10
p-nitrophenyl phosphate	67	104	122	73
Glucose-6-phosphate	<10	12	<10	<10
Ribose 5-phosphate	36	80	78	34
Pyridoxal-5-phosphate	<10	19	<10	<10
Adenosine triphosphate	<10	22	<10	<10
Adenosine diphosphate	<10	53	22	25

Note: The substrates were present at a concentration of 1 mM, and the released orthophosphate was quantified using the Malachite Green kit, as described under *Experimental Procedures*. Three independent assays were conducted, and the reported values represent the average of these assays, with a standard deviation below 15% of the reported values.

plots (Table 3). Additionally, K_{cat} values were calculated. For physiological substrates such as 5'-AMP, 5'-UMP, and 5'-GMP, the K_m values remained consistent across temperature and pH, ranging between 160 and 300 μ M. The K_{cat} values for these substrates ranged from 70 to 160 s^{-1} , while the efficiency rate (K_{cat}/K_m) showed values averaging from 325 to 498 (M/s), regardless of pH or temperature (Table 3).

In contrast, the efficiency value of FS6 with PNPP was over two orders of magnitude lower than with physiological substrates due to a low turnover rate with this colorimetric substrate. Interestingly, at 25°C, FS6 exhibited higher affinity for PNPP than at 50°C, whereas K_{cat} values displayed the opposite trend, as expected.

To determine the reaction enthalpies of FS6 acid phosphatase with the three physiological substrates (5'-GMP, 5'-AMP, and 5'-UMP) and the artificial substrate PNPP, we measured the heat flow (μ cal s^{-1}) over time using an ITC (Beezer et al., 1974). Injection of each substrate resulted in an exothermic reaction (Figure S2). Integration of the curve area, minus the

heat associated with the dilution event during substrate injection, provided ΔH (KJ/mol) values ranging from -2.69 ± 0.01 to -24.2 ± 0.03 KJ/mol at pH 5.5 and 7.5 (Table 4), indicating the exothermic nature of the enzymatic reactions.

Catalytically inactive mutants

The 3D structure of several class C acid phosphatases reveals their dimeric nature and the presence of 11 alpha-helices and 6/7 beta strands (Figure S3) (Felts et al., 2006, 2007; Singh et al., 2009, 2011). Through multiple alignment of amino acid sequences among type C bacterial phosphatases, it was found that these proteins possess two motifs within a bipartite signature motif (Thaller et al., 1997; Reilly et al., 2009; Neal et al., 2018). The first motif, located near the N terminus, consists of (I/V)-(V/A/L)-D-(I/L)-D-E-T-(V/M)-L-X-(N/T)-XX-Y. The second motif, located near the C terminus, is (I/V)-(L/M)-XX-G-D-(N/T)-L-X-D-F. These

TABLE 3 Kinetic parameters at different pH and temperatures determined by spectrophotometric technique.

	pH	Temperature (°C)	pNPP			AMP-5'			GMP-5'			UMP-5'		
			Km (mM)	Vmax (M/s)	Kcat (s ⁻¹)	Km (mM)	Vmax (M/s)	Kcat (s ⁻¹)	Km (mM)	Vmax (M/s)	Kcat (s ⁻¹)	Km (mM)	Vmax (M/s)	Kcat (s ⁻¹)
pH 4	25°C	0.31±0.16	1.37E-07± 7.15E-08	0.1±0.08	0.23±0.06	1.04E-04± 5.33E-05	75.67±26.10	0.18±0.02	7.55E-05± 2.05E-05	75±20.22	0.17±0.04	6.98E-05± 1.18E-05	69.67±11.85	
		50°C	n.d	n.d	n.d	n.d	n.d	n.d	n.d	n.d	n.d	n.d	n.d	
pH 5.5	25°C	0.04±0.01	7.14E-08± 2.03E-08	0.07±0.02	0.18±0.07	8.40E-05± 2.86E-05	83.67±29.16	0.22±0.02	1.07E-04± 1.88E-05	106.67±18.5	0.18±0.13	1.01E-04± 3.94E-05	100.33±39.8	
		50°C	0.17±0.06	2.38E-08± 1.36E-08	0.02±0.02	0.20±0.11	8.87E-05± 5.07E-05	88.67±50.64	0.17±0.05	7.82E-05± 1.08E-05	78.33±10.69	0.36±0.04	1.61E-04± 1.91E-05	161±19.47
pH 7	25°C	0.02±0	7.81E-08± 3.03E-08	0.07±0.03	0.20±0.01	9.30E-05± 1.16E-05	92.33±11.93	0.26±0.03	1.20E-04± 8.96E-06	119.67±8.39	0.19±0.07	9.56E-05± 2.33E-05	95±24.27	
		50°C	0.18±0.02	2.74E-08± 1.32E-08	0.02±0.02	0.36±0.08	1.39E-04± 1.57E-05	138.33±15.18	0.23±0.04	3.78E-04± 4.86E-04	95.33±4.93	0.20±0.02	9.15E-05± 1.99E-05	92.33±21.08
pH 8.5	25°C	0.05±0	1.95E-08± 3.32E-09	0.02±0.01	0.16±0.05	7.62E-05± 3.13E-05	76±31.48	0.25±0.08	1.18E-04± 2.36E-05	117.67±23.2	0.26±0.05	6.99E-05± 5.38E-05	116±41.94	
		50°C	0.19±0.04	1.67E-08± 9.33E-09	0.01±0.01	0.25±0.10	1.12E-04± 5.70E-05	150.33±44.50	0.16±0.01	8.08E-05± 3.65E-06	80.67±3.06	0.25±0.07	2.79E-04± 2.89E-04	97±43.55

TABLE 4 Exothermic reaction of FS6 with nucleoside monophosphate.

	ΔH (kJ/Mol)			
	PNPP	5'-AMP	5'-AMP	5'-UMP
pH 5.5	-7.62	-5.69	-5.89	-2.69
pH 7.5	-24.2	-15.6	n.d	n.d

The ITC assays were performed a minimum of three times as described under *Experimental Procedures* section. The ΔH (kJ/mol) values were determined based on the heat released during the completion of substrate hydrolysis. The values given are the averages from these assays, and the standard deviation falls within a the range of 10% of the given values.

motifs are separated by a polypeptide linker region of variable length (Thaller et al., 1997). Notably, the protein encoded by FS6 contains the characteristic bipartite sequence motif with L-D-I-D-E-T at residues 57–62 and G-D-N-L-G-D-F at positions 206 to 212. In the context of amino acid sequence conservation and secondary structure prediction, the role of the four aspartic acid residues (58, 60, 207, and 211) in the binding pocket is multifaceted. Asp 58 acts as a nucleophile, initiating the reaction by attacking the phosphorus (P) atom of the substrate, while Asp 60 functions as an acid, protonating the leaving group to facilitate its departure. Additionally, all four aspartic acid residues (58, 60, 207, and 211) contribute to the binding of a Mg²⁺ ion, further stabilizing the enzymatic complex.

Mutant forms of the enzyme were generated by substituting an aspartic acid residue by alanine of the DIDE motif at amino acid positions 58 and 60, and two other mutants were generated at the C-terminal DNLGD motif at amino acid positions 207 and 211 (Figure S4). These point mutants displayed no activity when using PNPP as a substrate. Since the mutated residues play a role in attacking the ester bond and in maintaining Mg²⁺ in the active site to establish appropriate bonds in the catalytic pocket, and given that FS6 is nearly 100 times more efficient with 5'-UMP than with PNPP, we also performed the tests using 5'-UMP as a substrate to determine if the mutants preserve some residual activity with this substrate. The obtained results revealed that all mutants were no active.

Molecular mass and oligomeric state of the FS6 protein

The monomeric molecular mass of FS6, determined by SDS-PAGE, closely matched its theoretical mass of approximately 38 kDa. To gain insights into the size and shape of the FS6 protein, analytical ultracentrifugation sedimentation studies were carried out. The ratio of the frictional coefficient of FS6 to the coefficient of friction of an ideal globular protein (f/f_0 ratio) was found to be 1.48. This suggests that FS6 is relatively globular in shape, with some elliptical characteristics. The

sedimentation coefficient, denoted as $S_{20,w}^0$, was determined using the methods described in the *Experimental Procedures* section and was found to have a value of 12.4. The sedimentation gradient analysis revealed that over 92% of the protein in the gradient corresponded to a single form (Figure 3 and Table 5). This allowed an estimation of the apparent molecular mass of the FS6 complex, which was approximately 372,000 Daltons. Taking into account that the monomer was 38kDa by SDS-PAGE, these results suggested that FS6 exists as a decamer in solution. This is in contrast to the typically

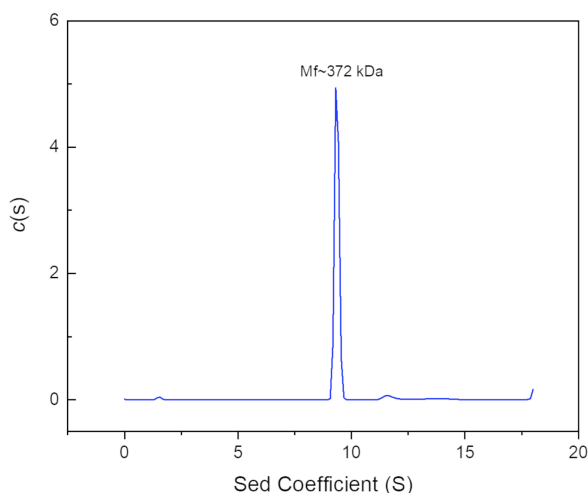


FIGURE 3 Sedimentation Velocity Analytical Ultracentrifugation of FS6. Sedimentation velocity analytical ultracentrifugation of FS6 assays were conducted at 20°C, using an AnTi50 rotor, under the specific conditions described in the *Experimental Procedures* section. The values represent the sedimentation velocity of FS6 under these conditions.

TABLE 5 Parameters of the ultracentrifugation sedimentation analysis.

	FS6
Peak	94.3%
sw (S)	9.354
sw (20,w) (S)	12.397
c	1.2819
% of total	92.319
Coefficient of friction (f/f_0)	1.4775
Mw (Da)	371,632
vbar	0.73
vbar20	0.73
Hydration	0.3
Buffer density	1.2538
Relative viscosity	1.2285
Minimun Mw for compact sphere (Da)	201,327
Stokes Radius (20°C)	7.16
a/b(oblate)	7
a/b(prolate)	6.39

dimeric forms observed in solution and in crystallized acid phosphatases of class C, such as the enzyme from *Pasteurella multocida*, *Bacillus anthracis*, *Sphingobium* sp., and *Haemophilus influenzae* (Figure S3).

Given the unusually large size of FS6, the complex was visualized using ultra-high resolution electron microscopy with negative staining. The negatively stained protein exhibited an average size of 11 ± 1 nanometres and displayed a relatively globular shape, consistent with the findings from the ultracentrifugation data. According to Erickson, the specific volume of the protein was estimated to be 436 nm^3 . The above estimated diameter of the protein from electron microscopy is in agreement with Erickson's estimated minimal radius (R_{min}) for proteins with molecular masses ranging from 200 to 500 kDa (Erickson, 2009).

DISCUSSION

In several protein families, conserved sequence patterns exhibit high sequence identity regions that are limited to active sites, cofactor binding domains, or specific DNA binding regions (Gandhi & Chandra, 2012). However, Udaondo et al. (2020) discovered that 1500 different class C acid phosphatase sequences exhibited conserved motifs throughout the sequence. This observation was deduced from the consensus sequences derived from multiple alignments, which revealed scattered sequence conservation across the entire protein sequence. This indicates the presence of several functional constraint regions with a lower site-specific substitution ratio distributed along the protein sequences.

In this study, we compared the sequence of crystallized class C acid phosphatases that exhibit a similar fold and high conservation at the catalytic site with the FS6 sequence. By aligning the sequence of FS6 with the derived consensus sequence for class C acid phosphatases, we discovered that 44% of the globally conserved residues in the consensus are also present in FS6 (30% of the residues were identical, see Figure S1). Although we currently lack knowledge about the impact of other residues on the unique properties of the FS6 protein, we assume that variations in the non-conserved residues and its longer N-terminal end with respect to other proteins of the family may contribute to the thermophilic properties of FS6 and its functionality in a wide pH range.

FS6 demonstrates a preference for dephosphorylating 5'- and 3'-nucleoside phosphates, but it also exhibits relaxed substrate specificity. The kinetic parameters determined for FS6 indicate that the enzyme is more efficient with potential physiological substrates than with artificial ones. This phenomenon has been observed in various hydrolases of fungal origin (Daddaoua et al., 2023) and enzymes that attack plastic monomers (Lai et al., 2023; Lear

et al., 2021; Ren & Ni, 2023). However, the results with FS6 contrast with those obtained with another acid phosphatase extremozyme from *Thermus thermophilus* that exhibit the opposite behaviour (Tham et al., 2010). The purified FS6 exhibited a remarkable turnover number when tested with various physiological substrates ($70\text{--}170\text{ s}^{-1}$), and its K_m values were in the low mM range, similarly to the findings reported for enzymes derived from other microorganisms. Considering the high turnover rate of FS6 and comparable K_m values to enzymes from other sources, FS6 appears to be an efficient enzyme for biotechnological applications requiring hydrolysis of different phosphomonoesters, including 2'-, 3'-, and 5'-nucleoside monophosphates, amino acid phosphates, and ribose-5-phosphate. Furthermore, the higher catalytic efficiency of FS6 with 5'-nucleosides agrees with the binding of these substrates in an anti-conformation, whereas 3'-substrates assume a syn conformation, what is in agreement with results obtained with other class C acid phosphatases (Singh et al., 2010). Our results with PNPP revealed that K_m values were similar regardless of pH. This contrasts with the *Clostridium* enzyme, whose affinity decreases as the pH increases. Another contrast with the *Clostridium* enzyme is that FS6 is more efficient with physiological substrates than with PNPP (Reilly et al., 2009). Overall, it seems that the FS6 enzyme shows pH-independent K_m values with PNPP, contrasting with the pH-dependent behaviour observed for the *Clostridium* enzyme. Additionally, the FS6 enzyme showed greater efficiency with physiological substrates compared to PNPP, which differs from the *Clostridium* and *Sphingobium* enzyme's performance (Reilly et al., 2009; Rangu et al., 2022). While FS6 exhibits low identity with the *Thermus thermophilus* extremozyme, it functions effectively across a wide range pH and high temperatures. It should be noted that the *Thermus* enzyme displayed optimal temperature at 70°C .

Currently, our efforts are focused on crystallizing FS6, as the apparent oligomeric state suggests a possible decameric structure, in contrast to the dimeric form observed in previously crystallized proteins (Rangu et al., 2022; Felts et al., 2007; Singh et al., 2011 and Felts et al., 2006). Although the exact nature of subunit interactions remains unknown, it is worth mentioning that the rPmCCAP protein of *Pasteurella multocida* has been described as a trimer of dimers (Singh et al., 2011). Consequently, the decamer observed in FS6 could potentially be a pentamer of dimers. It should be noted that for the rPmCCAP enzyme, hexamer assembly has been observed during crystallization, and this was assumed to be a crystallization artefact associated to a set of interactions of the poly-histidine; this was proposed because removal of the tag resulted in a protein that

was dimeric in solution (Singh et al., 2011). Whether the multimeric stage of FS6 is due to interactions at the poly-histidine tag is unknown at present, but the FS6 is a decamer in solution. This together with potential applications of FS6 in formulations for fertilizers and as a food supplement for monogastric animals is under investigation in our laboratory.

AUTHOR CONTRIBUTIONS

Maria-Isabel Recio: Data curation (equal); formal analysis (equal); investigation (equal). **Jesús De la Torre:** Data curation (equal); formal analysis (equal); investigation (equal). **Estrella Duque:** Methodology (equal); supervision (equal); writing – original draft (equal). **Zulema Udaondo:** Software (equal). **ABDELALI DADDAOUA:** Data curation (equal); formal analysis (equal); methodology (equal). **José Antonio Gavira:** Formal analysis (equal); investigation (equal); methodology (equal). **Carmen López-Sánchez:** Methodology (supporting). **Juan L. Ramos:** Conceptualization (equal); data curation (equal); formal analysis (equal); funding acquisition (equal); supervision (equal); writing – original draft (equal); writing – review and editing (equal).

ACKNOWLEDGEMENTS

We thank Ben Pakuts and Tino Krell for critical reading of the manuscript. We thank servicio de interacciones moleculares from Centro de Investigaciones Biológicas Margarita Salas in Madrid for support with ultracentrifugation assays. Work in our laboratory is supported by grants from the Ministry of Science through grants from the Plan Nacional 2021 (PID2021-123469OBI00) and Transición Ecológica (TED2021129632BI00) and European Commission projects EJP soils (EJPSOIL862695) and PREPSOIL (HE/CL5SOILM/0102).

FUNDING INFORMATION

No funding information provided.

CONFLICT OF INTEREST STATEMENT

The authors declare no conflict of interest.

ORCID

Abdelali Daddaoua  <https://orcid.org/0000-0002-7348-6393>

Zulema Udaondo  <https://orcid.org/0000-0003-3445-6842>

Juan L. Ramos  <https://orcid.org/0000-0002-8731-7435>

REFERENCES

- Abadou, A. & Labdury, J.E. (2006) Survey of the year. 2004: literature on application of isothermal titration calorimetry. *Journal of Molecular Recognition*, 19, 79–89.
- Attwood, P.A.V. (2013) P-N bond protein phosphatases. *Biochimica et Biophysica Acta*, 2013(1834), 470–478.

- Beezer, A.E., Steenson, T.I. & Tyrrell, H.J.V. (1974) Application of flow-microcalorimetry to analytical problems. II. Urea-urease system. *Talanta*, 21, 467–474.
- Bianconi, M.L. (2003) Calorimetric determination of thermodynamic parameters of reaction reveals different enthalpic compensations of the yeast hexokinase isozymes. *The Journal of Biological Chemistry*, 278, 18709–18713.
- Blank, L.M. (2023) (Poly) phosphate biotechnology: Envisaged contributions to a sustainable P future. *Microbial Biotechnology*, 16(8), 1616.
- Bonneau, L., Huguet, S., Wipf, D., Pauly, N. & Truong, H.N. (2013) Combined phosphate and nitrogen limitation generates a nutrient stress transcriptome favorable for arbuscular mycorrhizal symbiosis in *Medicago truncatula*. *New Phytologist*, 199, 188–202.
- Brown, P.H. & Schuck, P. (2008) A new adaptive grid-size algorithm for the simulation of sedimentation velocity profiles in analytical ultracentrifugation. *Computer Physics Communications*, 178, 105–120.
- Daddaoua, A., Álvarez, C., Oggerin, M., Rodríguez, N., Duque, E., Amils, R. et al. (2023) Rio Tinto as a niche for acidophilus enzymes of industrial relevance. *Microbial Biotechnology*, 16, 1069–1086.
- Dick, W.A., Cheng, L. & Wang, P. (2000) Soil acid and alkaline phosphatase activity as pH adjustment indicators. *Soil Biology and Biochemistry*, 32, 1915–1919.
- Du Plessis, E.M., Theron, J., Joubert, L., Lotter, T. & Watson, T.G. (2002) Characterization of a phosphatase secreted by *Staphylococcus aureus* strain 154, a new member of the bacterial class C family of nonspecific acid phosphatases. *Systematic and Applied Microbiology*, 25, 21–30.
- Erickson, H.P. (2009) Size and shape of protein molecules at the nanometer level determined by sedimentation, gel filtration, and electron microscopy. *Biological Procedures Online*, 11, 32–51.
- Felts, R.L., Ou, Z., Reilly, T.J. & Tanner, J.J. (2007) Structure of recombinant *Haemophilus influenzae* e (P4) acid phosphatase reveals a new member of the haloacid dehalogenase superfamily. *Biochemistry*, 46, 11110–11119.
- Felts, R.L., Reilly, T.J., Calcutt, M.J. & Tanner, J.J. (2006) Cloning, purification and crystallization of *Bacillus anthracis* class C acid phosphatase. *Acta Crystallographica. Section F, Structural Biology and Crystallization Communications*, 62(Pt 7), 705–708.
- Fernández, M., Rico-Jiménez, M., Ortega, Á., Daddaoua, A., García-García, A.I., Martín-Mora, D. et al. (2019) Determination of ligand profiles for *Pseudomonas aeruginosa* solute binding proteins. *International Journal of Molecular Sciences*, 20, 5156.
- Gandhi, U.N. & Chandra, B.S. (2012) A comparative analysis of three classes of bacterial non-specific acid phosphatases and archaeal phosphoesterases: evolutionary perspective. *Acta Informatica Medica*, 20, 167–173.
- Gottesman, M.E., Chudaev, M. & Mustae, A. (2020) Key features of magnesium that underpin its role as the major ion for electrophilic biocatalysis. *The FEBS Journal*, 287, 5439–5463.
- Kaur, P., Lingner, A., Singh, B., Böer, E., Polajeva, J., Steinborn, G. et al. (2007) APHO1 from the yeast *Arxula adenivorans* encodes an acid phosphatase of broad substrate specificity. *Antonie Van Leeuwenhoek*, 91, 45–55.
- Krell, T. (2008) Microcalorimetry: a response to challenges in modern biotechnology. *Microbial Biotechnology*, 1, 126–136.
- Lai, J., Huang, H., Lin, M., Xu, Y., Li, X. & Sun, B. (2023) Enzyme catalyzes ester bond synthesis and hydrolysis: the key step for sustainable usage of plastics. *Frontiers in Microbiology*, 13, 1113705.
- Lear, G., Kingsbury, J.M., Franchini, S., Gambarini, V., Maday, S.M.D., Wallbank, J.A. et al. (2021) Plastics and the microbiome: impacts and solutions. *Environmental Microbiomes*, 16, 2.
- Li, J., Xu, L. & Yang, F. (2007) Expression and characterization of recombinant thermostable alkaline phosphatase from a novel thermophilic bacterium *Thermus thermophilus* XM. *Acta Biochimica et Biophysica Sinica Shanghai*, 39, 844–850.
- Lidbury, I.D., Murphy, A.R., Scanlan, D.J., Bending, G.D., Jones, A.M., Moore, J.D. et al. (2016) Comparative genomic, proteomic and exoproteomic analyses of three *Pseudomonas* strains reveals novel insights into the phosphorus scavenging capabilities of soil bacteria. *Environmental Microbiology*, 18, 3535–3549.
- Lidbury, I.D., Scanlan, D.J., Murphy, A.R.J., Christie-Oleza, J.A., Aguilo-Ferretjans, M.A., Hitchcock, A. et al. (2022) A widely distributed phosphate-insensitive phosphatase presents a route for rapid organophosphorus remineralization in the biosphere. *Proceedings of the National Academy of Sciences of the United States of America*, 119, e2118122119.
- Margalef, O., Sardans, J., Fernández-Martínez, M., Molowny-Horas, R., Janssens, I.A., Ciais, P. et al. (2017) Global patterns of phosphatase activity in natural soils. *Scientific Reports*, 7, 1337.
- Margalef, O., Sardans, J., Maspons, J., Molowny-Horas, R., Fernández-Martínez, M., Janssens, I.A. et al. (2021) The effect of global change on soil phosphatase activity. *Global Change Biology*, 27, 5989–6003.
- Mitić, N., Smith, S.J., Neves, A., Guddat, L.W., Gahan, L.R. & Schenk, G. (2006) The catalytic mechanisms of binuclear metallohydrolases. *Chemical Reviews*, 106, 3338–3363.
- Neal, A.L., Blackwell, M., Akkary, E., Guyomer, C., Clark, I. & Hirsch, P.R. (2018) Phylogenetic distribution, biogeography and effects of land management upon bacterial non-specific acid phosphatase gene diversity and abundance. *Plant and Soil*, 427, 175–189.
- Philo, P.H. (2023) SEDNTERP: a calculation and database utility to aid interpretation of analytical ultracentrifugation and light scattering data. *European Biophysics Journal*, 52, 233–266.
- Ramos, J.L. (2022) Extremophile enzymes for food additives and fertilizers. *Microbial Biotechnology*, 15, 81–83.
- Rangu, S.S., Singh, R., Gaur, N.K., Rath, D., Makde, R.D. & Mukhopadhyaya, R. (2022) Isolation and characterization of a recombinant class C acid phosphatase from *Sphingobium* sp. RMS strain. *Biotechnology Reports*, 33, e00709.
- Reilly, T.J., Chance, D.L., Calcutt, M.J., Tanner, J.J., Felts, R.L., Waller, S.C. et al. (2009) Characterization of a unique class C acid phosphatase from *Clostridium perfringens*. *Applied and Environmental Microbiology*, 75(11), 3745–3754.
- Ren, S.-Y. & Ni, H.-G. (2023) Biodeterioration of microplastics by bacteria isolated from mangrove sediment. *Toxics*, 11, 432.
- Rigden, D.J., Bagyan, I., Lamani, E., Setlow, P. & Jedrzejak, M.J. (2001) A cofactor-dependent phosphoglycerate mutase homolog from *Bacillus stearothermophilus* is actually a broad specificity phosphatase. *Protein Science*, 10(9), 1835–1846.
- Rossolini, G.M., Schippa, S., Riccio, M.L., Berlutti, F., Macaskie, L.E. & Thaller, M.C. (1998) Bacterial nonspecific acid phosphohydrolases: physiology, evolution and use as tools in microbial biotechnology. *Cellular and Molecular Life Sciences CMLS*, 54, 833–850.
- Shi, W., Xing, Y., Zhu, Y., Gao, N. & Ying, Y. (2022) Diverse responses of *pqqC*- and *phoD*-harbouring bacterial communities to variation in soil properties of Moso bamboo forests. *Microbial Biotechnology*, 15, 2097–2111.
- Singh, H., Felts, R.L., Schuermann, J.P., Reilly, T.J. & Tanner, J.J. (2009) Crystal structures of the histidine acid phosphatase from *Francisella tularensis* provide insight into substrate recognition. *Journal of Molecular Biology*, 394, 893–904.
- Singh, H., Malinski, T.J., Reilly, T.J., Henzl, M.T. & Tanner, J.J. (2011) Crystal structure and immunogenicity of the class C acid phosphatase from *Pasteurella multocida*. *Archives of Biochemistry and Biophysics*, 509, 76–81.

- Singh, H., Schuermann, J.P., Reilly, T.J., Calcutt, M.J. & Tanner, J.J. (2010) Recognition of nucleoside monophosphate substrates by *Haemophilus influenzae* class C acid phosphatase. *Journal of Molecular Biology*, 404, 639–649.
- Studier, F.W., Daegelen, P., Lenski, R.E., Maslov, V. & Kim, J.F. (2009) Understanding the differences between genome sequences of *Escherichia coli* B strains REL606 and BL21(DE3) and comparison of the *E. coli* B and K-12 genomes. *Journal of Molecular Biology*, 394, 653–680.
- Thaller, M.C., Schippa, S., Bonci, A., Cresti, S. & Rossolini, G.M. (1997) Identification of the gene *aphA* encoding the class B acid phosphatase/phosphotransferase of *Escherichia coli* MG1655 and characterization of its product. *FEMS Microbiology Letters*, 146, 191–198.
- Tham, S., Chang, C.-D., Huang, H., Lee, Y., Huang, T. & Chang, C.-C. (2010) Biochemical characterization of an acid phosphatase from *Thermus thermophilus*. *Bioscience, Biotechnology, and Biochemistry*, 74, 727–735.
- Todd, M.J. & Gomez, J. (2001) Enzyme kinetics determined using calorimetry: a general assay for enzyme activity. *Analytical Biochemistry*, 296, 179–187.
- Udaondo, Z., Duque, E., Daddaoua, A., Caselles, C., Roca, A., Pizarro-Tobias, P. et al. (2020) Developing robust protein analysis profiles to identify bacterial acid phosphatases in genomes and metagenomic libraries. *Environmental Microbiology*, 22, 3561–3571.
- van Etten, R.L. (1982) Human prostatic acid phosphatase: a histidine phosphatase. *Annals of the New York Academy of Sciences*, 390(1), 27–51.
- van Etten, R.L. & Waymack, P.P. (1991) Substrate specificity and pH dependence of homogeneous wheat germ acid phosphatase. *Archives of Biochemistry and Biophysics*, 288, 634–645.
- Wang, Z., Tan, X., Lu, G., Liu, Y., Naidu, R. & He, W. (2018) Soil properties influence kinetics of soil acid phosphatase in response to arsenic toxicity. *Ecotoxicology and Environmental Safety*, 147, 266–274.
- Zambelli, B. (2019) Characterization of enzymatic reactions using ITC. *Microcalorimetry of Biological Molecules: Methods and Protocols*, pp. 251–266.
- Zhao, H., Brown, P.H., Balbo, A., Fernández-Alonso, M.C., Polishchuck, N., Chaudhry, C. et al. (2010) Accounting for solvent signal offsets in the analysis of interferometric sedimentation velocity data. *Macromolecular Bioscience*, 10, 736–745.

SUPPORTING INFORMATION

Additional supporting information can be found online in the Supporting Information section at the end of this article.

How to cite this article: Recio, M.-I., de la Torre, J., Daddaoua, A., Udaondo, Z., Duque, E., Gavira, J.A. et al. (2024) Characterization of an extremophile bacterial acid phosphatase derived from metagenomics analysis. *Microbial Biotechnology*, 17, e14404. Available from: <https://doi.org/10.1111/1751-7915.14404>